Tip Dependence of the Self-Assembly in Dip-Pen Nanolithography

Dong Min Heo,[†] Mino Yang,*[,†] Hyojeong Kim,[‡] Leton Chandra Saha,[‡] and Joonkyung Jang*[,‡]

Department of Chemistry, Chungbuk National University, Cheongju 361-763, Republic of Korea, and Department of Nanomaterials Engineering, Pusan National University, Miryang 627-706, Republic of Korea

Received: April 8, 2009; Revised Manuscript Received: June 8, 2009

In dip-pen nanolithography (DPN), an atomic force microscopy tip delivers molecules to the substrate and generates a self-assembled monolayer (SAM) with a nanometer resolution. Given the tip changes from experiment to experiment, it is important to know how DPN is affected by the change in the tip. In principle, a change in the tip can alter the initial conditions and the subsequent dropping of molecules from the tip to the substrate. The present molecular dynamics simulation compares DPN results obtained from two different tips, a quill type spherical tip and a cylindrical tip like a fountain pen. We investigate how the nanodroplet created under the tip spreads out to form a SAM on a goldlike substrate. For the early stage of DPN studied here (less than 1.5 ns), we find that a substantial variation in the tip does not yield any significant change in DPN. For a strong molecular binding to the substrate in particular, a SAM is entirely determined by the molecule−substrate binding energy, not by the detailed geometry of the tip. The dynamic features of growth in the SAM are also similar for both tips.

I. Introduction

In dip-pen nanolithography (DPN), an atomic force microscope (AFM) tip serves as a source of molecules that are designed to bind to a substrate. Because of the continuous downward flow of molecules, a multilayered droplet forms under the tip (Figure 1). As molecules in the upper layers step down to the bare substrate, the droplet spreads and the periphery of SAM broadens on the substrate. DPN proves to be a versatile tool for creating self-assembled monolayers (SAMs) on various substrates.[1−3] It finds numerous applications in biochips, nanomaterials, and the semiconductor industry.[1−3] In contrast to its wide applications, our understanding for the molecular details of DPN is far from complete. The molecular study of DPN is expected to be useful for assessing the possibility and limitation of DPN. DPN also covers various fundamental scientific phenomena such as capillary condensation of nanoscale water, self-assembly, and surface diffusion.

So far, theoretical and fundamental studies of DPN[4−16] have been mostly phenomenological[4,6−14] and have focused on the water meniscus which is formed at the end of the tip under humid conditions.[5,15,16] Only recently, we have reported molecular dynamics (MD) simulations for the growth of SAMs in DPN.[17,18] Adopting a coarse-grained model for octadecanethiol (ODT), we have examined the growth of SAMs by using a cylindrical tip containing molecules inside, mimicking the "nano-fountain pen" in experiment.[19] Our work showed that the SAM grows mainly through a serial pushing mechanism (Figure 1): A molecule dropped from the tip pushes out a molecule below, and the molecule pushed out in turn pushes one of its neighboring molecules out of place. As this push-induced displacement propagates from center to periphery, the SAM grows in size. The rising question for the serial pushing is in what direction a molecule moves when it is pushed by another molecule. Two limits can be considered. In the directionally coherent limit of serial pushing, each push-induced movement takes the same direction as the direction of initial pushing. In the opposite limit of directionally incoherent serial pushing, consecutive push-induced movements are uncorrelated and random in direction. Alternative to the serial pushing is the hopping down where molecules move on top of the bottom layer, reach the periphery, and then hop down to the bare substrate (Figure 1). This hopping down event is observed in simulations of a small-sized SAM. In general, the contribution of the hopping down mechanism to the SAM growth is minor.

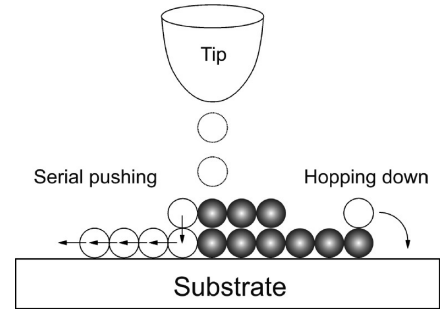

Figure 1. Growth mechanism of the SAM in DPN. Because of the molecular flow from the tip, a multilayer droplet forms under the tip. In the serial pushing mechanism (left), a molecule in the upper layer pushes the molecule below out of its place, and the molecule pushed out in turn pushes a molecule next to it, and so on. The arrows pointing toward the left represent the moving directions of the molecules pushed. In this case, four molecules on the substrate (drawn as open circles at the bottom) move due to the pushing initiated by the molecule in the second layer (open circle with an arrow downward). The monolayer can also grow by hopping down of a molecule (right). In the hopping down event, a molecule reaches the periphery by stepping over molecules of the bottom layer and then hops down to the substrate.

In DPN, the shape of the tip affects the initial positions of molecules and how molecules transfer to the substrate. Despite its vital role, the exact geometry of the tip is not known in experiment. Given the tip changes from experiment to experiment, it is important to know how sensitively DPN responds to the change in the tip. We are especially interested in how the

* To whom correspondence should be addressed. E-mail: minoyang@chungbuk.ac.kr (M.Y.) and jkjang@pusan.ac.kr (J.J.).
[†] Chungbuk National University.
[‡] Pusan National University.

10.1021/jp903254p CCC: $40.75
Published on Web 07/01/2009

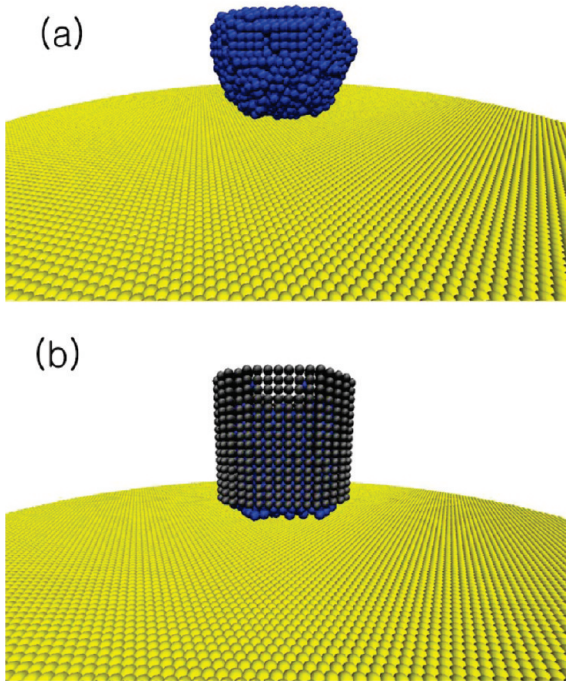

Figure 2. Molecular configurations for the two tips simulated. (a) A spherical tip. A total of 2097 molecules are coated on the hemispherical shell of 914 silicon-like atoms. Our Au (111)-like substrate is a single layer consisting of 17503 atoms. Molecules completely cover the outside of the tip, and the inside is covered mostly in the upper part of the tip. Therefore, tip atoms are not shown in the viewpoint of the figure. (b) A cylindrical tip. It is made of 1152 atoms and contains 2557 molecules inside. Some molecules stick out of the bottom end of the cylindrical tip. The substrate is the same as for the spherical tip.

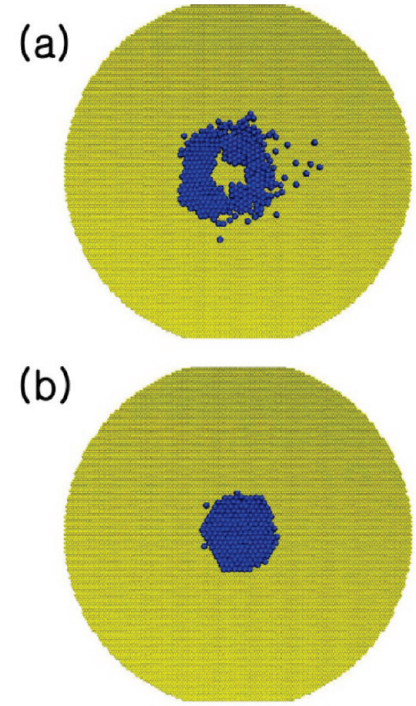

Figure 3. Area of molecular dropping for the spherical and cylindrical tips. We show molecules located in the second layer of the droplet under the tip for the spherical (a) and cylindrical (b) tips. The snapshot is taken at 500 ps, and the molecule−substrate binding energy is $\varepsilon_b/\varepsilon_0 = 2$.

change of the tip influences the growth dynamics and overall structure of SAM. To address these questions, it seems natural to compare DPN results from two different tips and investigate qualitative and quantitative differences. Herein, we present MD simulations of DPN for a spherical tip and a cylindrical tip. The spherical tip is coated with molecules, emulating a conventional quill type tip (Figure 2a). Our cylindrical tip mimics a nanofountain pen, which contains molecules inside (Figure 2b). These two tips significantly differ in shape and in the area of molecular dropping (Figure 3). As compared with the cylindrical tip, the spherical tip drops molecules over a wider area, and its dropping is less isotropic. Except for the present and previous work of ours,[17,18] we are not aware of any MD simulation that explicitly takes into account the presence of the tip in DPN. In addition, the present work simulates a conventional quill type tip, which has not been modeled so far.

Because of the disparate time scales of simulation (order of nanoseconds) and experiment (order of seconds), we do not attempt any quantitative reproduction of a specific experiment. A quantitative comparison is also hampered by the experimental uncertainty about the geometries of tip and substrate. Therefore, the present MD simulation focuses on the early stage of DPN (times less than 1.5 ns), which creates a SAM similar to the monolayer of ODT on Au (111). Instead of concentrating on a specific system, we explore a range of systems by systematically varying the binding energy between molecule and substrate (which we believe is the fundamental molecular parameter of DPN). Our simulation reveals the dynamics and mechanism for the growth of SAMs. We explain the shape of SAMs in terms of the substrate anisotropy, the directional coherence in the serial pushing, and the molecule−substrate binding energy. We quantitatively compare the radii of SAMs obtained from both tips. All of the analyses of MD simulation are given in section III. Section II gives a brief description of simulation method. We conclude in section IV.

II. Simulation Details

We model the spherical AFM tip as a hemispherical shell (3.4 nm in radius) made of 914 silicon-like atoms (Figure 2a). A total of 2097 molecules (drawn as spheres) are initially adsorbed on the tip surface. We also simulate a cylindrical tip (consisting of 1152 silicon atoms), which contains a total of 2557 molecules inside. The substrate for both tips is a single layer of a Au (111)-like surface consisting of 17503 atoms. The boundary of the substrate is a circle with a lateral diameter of 80 nm. The vertical distance from the tip end to the substrate is 1.37 nm for the spherical tip and 1.30 nm for the cylindrical tip. We run the simulation after adding molecules to the tip (see below). What matters most in the simulation is the closest approach of the molecule to the substrate. The closest approach is nearly identical for both tips (0.50 and 0.48 nm for the spherical and cylindrical tips, respectively). Except for the tip geometry described above, our simulation method is similar to the previous work, which contains more details.[18] The molecules are taken to be spherical in shape and have a mass of ODT [$CH_3(CH_2)_{17}SH$]. Every interatomic interaction is described by a Lennard−Jones (LJ) potential, $U(r) = 4\varepsilon[(\sigma/r)^{12} - (\sigma/r)^6]$, where r is the interatomic distance and σ and ε are the distance and energy parameters intrinsic to each atom.[20] The LJ parameters ε and σ for the tip atom are 0.4184 kJ/mol and 0.4 nm, respectively.[21] The LJ parameter ε of our molecule (=5.24 kJ/mol) is set identical to that of stearic acid ethyl ester, which is similar to ODT in mass.[22] We chose the LJ parameter σ of our molecule (=0.497 nm) to reproduce the experimental structure of ODT monolayer on Au (111).[23] The LJ σ of the substrate atom is that of the Au atom reported in the literature

(0.2655 nm).[24] We, however, systematically vary ε of the substrate atom to examine the effects of the molecule−substrate binding energy ε_b. We use the Lorentz−Berthelot combination rule[20] for the LJ interactions between different atomic species. The smallest value of ε_b, called ε_0, is set to 3.1 kcal mol^{-1}, which is close to the previous theoretical estimate of Au-ODT binding energy (3.182 kcal mol^{-1}).[25] We have considered additional values of ε_b as $\varepsilon_b/\varepsilon_0$ =1.4, 2.0, 2.8, 4, 5.7, 8.0, and 11.3. The case of $\varepsilon_b/\varepsilon_0 = 1$ in our simulation can be related to the case of ODT on gold substrate. Because our model does not take into account the molecular chemisorption on the substrate, the current simulation is expected to underestimate the interaction strength between ODT and gold. Also, because of the fact that the substrate in simulation is a single layer of gold atoms (instead of multilayers), the molecular attraction to the substrate is further underestimated. Therefore, we expect $\varepsilon_b/\varepsilon_0$ for ODT on gold is higher than 1. A precise determination of the value of $\varepsilon_b/\varepsilon_0$ corresponding to experiment seems difficult because our model lacks the chemisorption interaction and is highly coarse grained. We have shown, however, that our coarse-grained model captures the essence of an MD simulation, which takes into account the chain structure of ODT and the chemical bonding between gold and sulfur atoms.[17] Moreover, as mentioned in the Introduction, we are interested in studying DPN for a range of binding energies between molecule and substrate. We then examine a qualitative behavior of DPN with respect to the change in binding energy.

Before the start of the simulation for the spherical tip, we placed molecules at the cubic lattice points near the tip. Then, we increased ε of the tip atom by 100 times its original value and ran the MD simulation for 300 ps. Because of the enhanced tip attraction, molecules spontaneously adhere to the tip surface. The final configuration of such a preliminary run is shown in Figure 2a and serves as the initial condition for the main MD simulation. Some molecules stick to the upper part of the inner shell of the spherical tip. In the viewpoint of Figure 2a, the tip looks completely covered with molecules. For the cylindrical tip, we put molecules inside the cylinder and equilibrated the molecules by running an MD simulation for 500 ps. We then cut the bottom part of the cylinder so that some molecules stick out from the end of cylinder (Figure 2b). The tip and substrate atoms are taken to be rigid during the simulation. We use the velocity Verlet algorithm[20] with a time step of 3 fs. The total length of simulation was 1.5 ns. The temperature was set to 300 K by using a Berendsen thermostat.[26]

III. Results and Discussion

Graphic visualization of the simulation shows that a multilayer droplet constantly forms near the center of the SAM. The droplet looks like a circular pillar of molecular layers, which decreases its height as time goes by. The pillar for the cylindrical tip is straight from the bottom up. The pillar for the spherical tip has a narrow bottom relative to the top, and it is not so symmetric when viewed along the pillar axis. Typical molecular dropping areas for the spherical and cylindrical tips are shown in Figure 3. Molecules in the figure are actually located in the second layer of the droplet. Each snapshot is taken at 500 ps, and the binding energy is $\varepsilon_b/\varepsilon_0 = 2$. Notice that the area of molecular dropping is annular for the spherical tip (Figure 3a) but circular for the cylindrical tip (Figure 3b). The dropping area for the spherical tip is circular at times earlier than in Figure 3a (not shown). By the time of the snapshot, however, molecules dropped inside of the annulus pushed molecules below and became a part of the bottom layer. The dropping area is wider and less symmetrical for the spherical tip, giving rise to a SAM less symmetrical than that of the cylindrical tip (see below). There are some scattered molecules separated from the main island due to the molecular diffusion on top of the bottom layer.

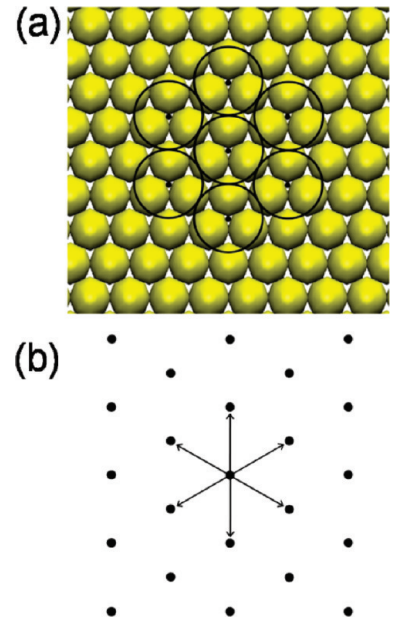

Figure 4. Three-fold hollow sites of the substrate and the trigonal lattice made of hollow sites. (a) Molecules (open circles) preferentially occupy the 3-fold hollow sites (dots) of Au (111)-like substrate. (b) The 3-fold hollow sites constitute a trigonal lattice (drawn as dots). The molecular movement on the substrate can be modeled as a series of jumps between adjacent lattice points. A molecule can jump toward one of six equivalent nearest neighbor points (drawn as arrows).

Our substrate has a hexagonal symmetry similar to that of Au (111). Molecules preferentially adsorb to one of 3-fold hollow sites of the substrate (Figure 4a). These hollow sites form a trigonal lattice as shown in Figure 4b. We can think of the molecular movement on the substrate (whether it is induced by push or voluntary) as a series of jumps between neighboring sites of the lattice (as in a random walk model). There are six equivalent directions available for a molecular jump from its current lattice position to its neighboring sites (Figure 4b). We find that this site-to-site jump is a good approximation of the molecular motion on the substrate. We will later use this description to explain the SAM growth.

By visual inspection of MD trajectories, we conclude that the SAM grows primarily through the serial pushing mechanism for both the spherical and the cylindrical tips. Typically, a molecule dropped on top of the bottom layer soon pushes a molecule below and touches the bare substrate. For a relatively small SAM, some molecules arrive at the periphery of the SAM by moving on top of the bottom layer and then hop down to the bare substrate. As the SAM grows in size, it takes more time and distance for a molecule to hop down because the periphery is far from the center of the SAM. Consequently, molecules on top of the bottom layer opt to push molecules below. The hopping down event then disappears, and the SAM grows entirely through the serial pushing mechanism.

Figure 5 illustrates the growth of a SAM for the spherical tip (with an intermediate binding energy, $\varepsilon_b/\varepsilon_0 = 2.8$) by showing four different snapshots of molecules touching the substrate. The SAM is circular and isotropic at early times ($t =$ 200 ps, Figure 5a). The SAM becomes hexagonal within 500 ps (Figure 5b). As time increases to 1 (Figure 5c) and 1.5 ns (Figure 5d), the periphery of the SAM develops six distinct

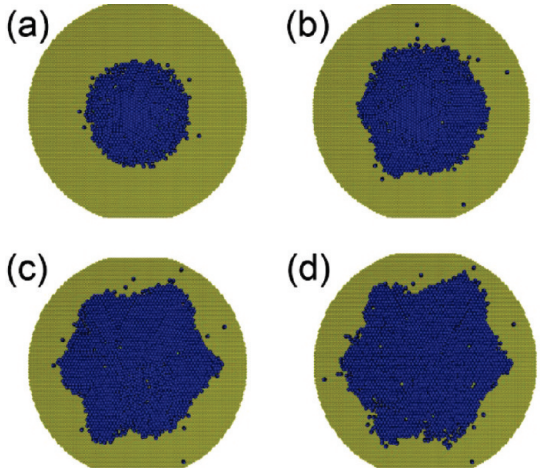

Figure 5. Growth of a SAM in simulation. Shown are the representative snapshots for $\varepsilon_b/\varepsilon_0 = 2.8$. The snapshots are taken, respectively, at $t = 200$ ps (a), 500 ps (b), 1 ns (c), and 1.5 ns (d). Shown are molecules in direct contact with the substrate.

branches with a hexagonal symmetry. To explain, we assume (to a good approximation) that molecules on the substrate move discretely on the trigonal lattice shown in Figure 4b. If pushed, a molecule jumps from its current position to one of six neighboring sites. If the serial pushing is directionally incoherent, each push-induced movement of molecule directs from its current position toward one of six neighboring positions with equal probability. The resulting SAM is circular in shape, and it is confirmed by performing a random walk simulation on the trigonal lattice. If the serial pushing is coherent in direction, however, a pushing originated at the center propagates in one direction all the way to the periphery. In the case of a point source (dropping one molecule each time at the center of SAM), the resultant SAM would be a hexagonal cross of molecular lines exuding from the center. In reality, the directional coherence is not perfect, and the tip has a circular area of molecular dropping (as in Figure 3). Instead of a hexagonal cross of narrow lines, the SAM has hexagonal shapes (with or without branches) as in Figures 5b−d. A similar behavior in the growth of SAM is found for the cylindrical tip with the same value of $\varepsilon_b/\varepsilon_0$ as in Figure 5 (not shown). The hexagonal branches of SAM for the cylindrical tip are more pronounced and symmetric. This is due to the fact that the molecular dropping for the cylindrical tip is more uniform and narrower than in the spherical tip (Figure 3b).

If the molecule−substrate binding is much weaker or stronger than in Figure 5, the hexagonal branches due to the directional coherence in pushing are not seen. Let us use the lattice description of molecular motion as in Figure 4. For a molecule that weakly binds to substrate, a molecule pushed out by another molecule can take any direction toward its nearest neighbors except toward the molecule pushing it. It is statistically less probable for consecutive push-induced movements to align in the same direction. As a result, the directional coherence does not show up, and a circular SAM forms. In the opposite case of strong molecule−substrate binding, the push of a molecule toward any direction becomes difficult. A push-induced displacement of molecule again tends to direct toward any of its nearest neighbors except toward the pushing molecule. The resulting SAM is circular for the same reason as for the case of a weak molecule−substrate binding. Only for some intermediate strength of molecule−substrate binding ($\varepsilon_b/\varepsilon_0 = 2.0$, 2.8, and 4 for the spherical tip and 4.0 and 5.7 for the cylindrical tip), the

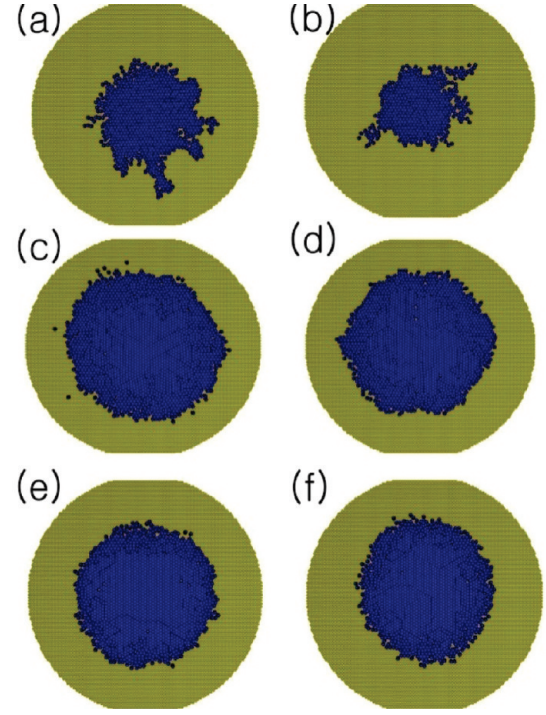

Figure 6. Tip dependence of the structure of SAM. Snapshots are taken at 1.5 ns. The final monolayer in the case of $\varepsilon_b/\varepsilon_0 = 1$ are shown in the top for the spherical (a) and cylindrical (b) tips. Figures in the middle (c and d) correspond to the spherical and cylindrical tips with $\varepsilon_b/\varepsilon_0 = 5.7$, respectively. The monolayer for a strong molecule−substrate binding, $\varepsilon_b/\varepsilon_0 = 11.3$, is shown in the bottom for the spherical (e) and cylindrical (f) tips, respectively.

directional coherence shows up as a hexagonal SAM with or without branches. In these particular cases, the deviation of a subsequent pushing from the initial pushing direction (along one of six directions in Figure 4b) seems to be opposed by molecules that do not lie along the line of the initial pushing direction.

Figure 6 compares the SAMs obtained by using the spherical (parts a, c, and e) and cylindrical (parts b, d, and f) tips. Drawn are the snapshots taken at the final time of simulation (1.5 ns) for three different values of ε_b. The shape of SAM is similar for both tips, especially for large ε_b($\varepsilon_b/\varepsilon_0 = 11.3$, Figures 6e,f). As ε_b increases, the SAM becomes independent of the shape of tip. This suggests that for molecules strongly bound to substrate, a consistent SAM should be obtained regardless of the tip. In the case of a small ε_b($\varepsilon_b/\varepsilon_0 = 1$), both tips give SAMs with random (in direction and length) branches. The SAM for the spherical tip is bigger. The directional coherence in the serial pushing is absent because molecules easily move between the trigonal lattice sites of substrate (Figure 4b). The SAM is not a compact circle because its periphery rearranges as time goes by (however, the main body of SAM remains intact). As ε_b increases, the irregular branches of SAM disappear, and the SAM becomes compact (Figure 6c−f). The SAM does not show any significant voluntary rearrangement in periphery as for small ε_b. For an intermediate binding energy, $\varepsilon_b/\varepsilon_0 = 5.7$ (Figure 6c,d), the SAM is hexagonal for both tips due to the directional coherence in the serial pushing. In the case of a strong molecule−substrate binding energy (parts e and f), SAMs for both tips are quite circular and very similar to each other. Here, the molecular movement on the substrate requires more energy than before because it requires pushing out molecules strongly bound to the substrate. Now, the collective movement of molecules in the same direction (directionally coherent serial

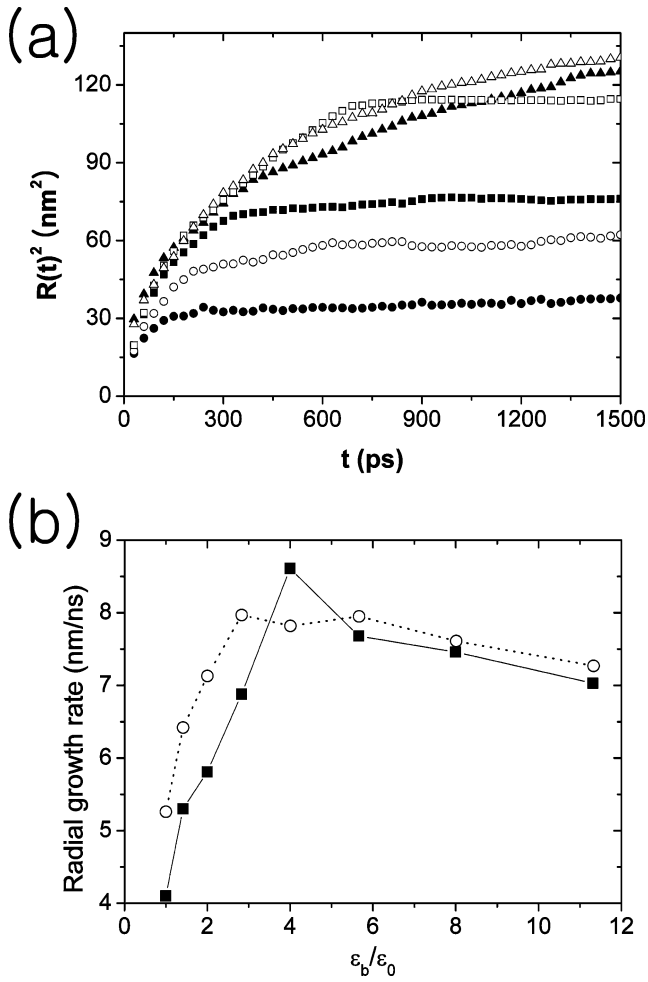

Figure 7. (a) Radial growth of the monolayer for various binding energies between molecule and substrate ε_bs. We plot the radius squared, $R(t)^2$ vs time t for $\varepsilon_b/\varepsilon_0 = 1$ (circles), 2 (squares), and 4 (triangles). $\varepsilon_0 = 3.1$ kcal mol^{-1}. $R(t)^2$ is drawn as filled (open) symbols for the cylindrical (spherical) tips, respectively. (b) The radial growth rate vs the molecule−substrate binding energy. The radial growth rate is defined as the radius divided by time $R(t)/t$ at $t = 1.5$ ns and is plotted as a function of $\varepsilon_b/\varepsilon_0$. The growth rates for the cylindrical and spherical tips are drawn as filled squares and open circles, respectively. Lines are drawn as a visual guide.

pushing) becomes difficult. As a result, the SAM growth becomes isotropic, giving a circular periphery.

We kept track of the radius of SAM, $R(t)$, in time by checking the number of molecules belonging to the main island at time t. The radius squared $R(t)^2$ is taken to be that number divided by $\pi\rho$, where ρ is the density of a perfect SAM on the substrate. In Figure 7a, we present $R(t)^2$ as a function of t for the spherical (open symbols) and cylindrical (filled symbols) tips. We varied ε_b as $\varepsilon_b/\varepsilon_0 = 1$ (circles), 2 (squares), and 4 (triangles). All in all, the radial growth shows a similar behavior for both tips. The figure shows two distinct phases in the growth of SAM. In the initial launching phase[18] (approximately times less than 200 ps), molecules flow down relatively fast from the tip and move on the substrate without strong resistance of molecules preoccupying the substrate. The launching phase persists until the area directly under the tip is completely covered with molecules. The radial growth of SAM is diffusional in its time dependence ($R \propto t^{1/2}$). After the launching phase, the nascent SAM around the tip expands slowly. This was previously named the expansion phase.[18] The slope of $R(t)^2$ with respect to t significantly decreases in the expansion phase as compared with that of the launching phase. Because the area near the tip is already covered with molecules, the growth of the SAM requires a long series of pushing that propagates to the periphery. Such a concerted motion of many molecules is slower than the molecular motion involving few molecules as in the pushing during the launching phase. $R(t)^2$ for the weak binding energy, $\varepsilon_b/\varepsilon_0 = 1$, sometimes decreases a little bit as time goes by. The SAM in this case fluctuates; therefore, molecular dropping does not always enlarge the size of the SAM. According to Figure 7a, roughly 2000 molecules are dropped within 1.5 ns for both tips. The corresponding molecular dropping rate is calculated to be about 10^{12} s^{-1}, which is nearly 10^7 times faster than the experimental rate for ODT on gold ($=4.2 \times 10^5$ s^{-1}).[4] This discrepancy arises from the fact that our time scale in the simulation is limited to short times as compared to the experimental time scale. Notice that the radius squared in Figure 7a increases very slowly at times later than the initial 300 ps. If we extend the time window in Figure 7a further out to an experimental time scale (seconds), the molecular dropping rate is expected to decrease drastically to the order of that observed in experiment.

As a measure of how fast the radius of the SAM grows in time, we calculated the radial growth rate of the SAM defined as the value of $R(t)/t$ taken at $t = 1.5$ ns. Figure 7b shows how the radial growth rate depends on the molecule−substrate binding energy ε_b for each tip. The final radii for the spherical and cylindrical tips are drawn as open circles and filled squares, respectively. Regardless of the tip, the figure illustrates a nonmonotonic behavior of the growth rate with respect to ε_b. Up to a certain value of binding energy ($\varepsilon_b/\varepsilon_0 = 2.7$ for the spherical tip and $\varepsilon_b/\varepsilon_0 = 4.0$ for the cylindrical tip), increasing ε_b increases the radial growth rate of the SAM. An enhanced attraction of the substrate makes molecules flow down from the tip faster and form a larger SAM within a given amount of time. A further increase in ε_b, however, makes the radial growth slower. Because of a very strong molecular binding to the substrate, molecules on the substrate are less mobile than for a smaller ε_b. The serial pushing of molecules from the center toward the periphery is severely retarded by molecules strongly attached to the substrate. Therefore, the radial growth rate decreases for an extremely large ε_b. Notice that the growth rate for the two tips converges to a common value as ε_b increases, starting from $\varepsilon_b/\varepsilon_0 = 5.7$.

IV. Concluding Remarks

Despite the widespread use of DPN in application, we poorly understand the molecular events underlying DPN. Given that an AFM tip is responsible for molecular delivery and nanometer resolution of DPN, it is interesting to see how DPN is influenced by the change in the tip. Herein, we have performed MD simulations to study the growth of the SAM by using two different tips. A quill type spherical tip (coated with molecules) is compared to a cylindrical tip similar to a fountain pen (holding molecules inside). Experimentally, it is desired to have a tip that gives well-controlled DPN features or faster deposition rates. The previous experimental study investigated the effect of tip size[27] or the number of molecules coated on the tip.[28] In contrast, the present work compares qualitatively different tips, a quill tip and a fountain pen tip, and such comparison has not been made before. The molecular dropping area and the initial conditions of molecules on the tip for the two tips differ significantly. Rather unexpectedly, the structure of the SAM does not depend much on the detailed geometry of the AFM tip. For a relatively weak molecule−substrate binding, the detailed structure of the SAM varies from tip to tip. The

qualitative characteristics of SAM (random branches), however, are the same regardless of tip. In the case of a strong molecular binding to the substrate, the change of the tip does not affect the structure of SAM.

The growth dynamics of SAM are similar for both the spherical and the cylindrical tips. The SAM grows primarily through the serial pushing mechanism. Molecules dropped from the tip push out molecules below, and molecules pushed out in turn push other molecules nearby. The SAM grows as such pushing propagates from the center to the periphery of the SAM. Depending on the molecule−substrate binding energy, consecutive push-induced movements sometimes align in the same direction as the initial direction (directionally coherent serial pushing). In other cases, each movement in the successive pushing is independent and random in direction (directionally incoherent serial pushing). The directional coherence manifests itself as a hexagonal SAM, which occasionally develops distinct 6-fold branches. The SAM grows through two phases in its time dependence, initially fast launching and then slow expansion phases. The growth of SAM becomes faster with raising the binding energy between molecule and substrate, reflecting the enhanced pull from the substrate. A further rise in the binding energy, however, slows down the growth because an extremely strong molecular binding to the substrate retards the propagation of molecular pushing from the center toward the periphery.

If a molecule weakly binds to the substrate, the SAM created in DPN is sensitive to the details of the tip geometry and how molecules are prepared initially. In this case, a reproducible SAM structure is not expected even if a single tip is used. More relevant to practical DPN would be the case where a molecule binds to the substrate strongly. Here, one can generate a consistent SAM by using a single tip. Our MD simulation shows further that nearly identical SAMs result even if we use tips with quite different shapes. In this case, the structure of SAM is solely determined by the intermolecular and molecule−substrate binding energies. Then, we can focus on the properties of the molecule and substrate, leaving out the detailed geometry of the tip and the initial configuration of molecules.

The present work shows that a stable SAM can be obtained even if molecules do not make any chemical bond with the substrate. Our LJ potentials for intermolecular and molecule−substrate interactions are enough to produce a stable SAM (for a large molecule−substrate binding energy). It is certainly desirable to include the chemisorption interaction for the thiol on the gold substrate. Unfortunately, the chemisorption potential is currently not well-established. In our simulation adopting a Morse potential for the chemisorption of the sulfur atom to gold, we have not seen any chemisorption event during the time scale of simulation (several nanoseconds). Maybe the chemisorption occurs with a time scale longer than the simulation time scale, or the Morse potential description is not good enough to model the chemisorption. A many-body reactive force field might be needed to describe the gold−surfur interaction accurately. There are some preliminary attempts to develop a reactive force field optimized against ab initio calculations and experiments.[29] Such a sophisticated force field, however, is probably too complicated to be implemented in a MD simulation, which typically involves tens of thousands of atoms at least. Once chemisorption is properly taken into account, molecules will stop moving outward once they adsorb chemically. This might contrast with the present simulation where molecules are continuously pushed away from the tip during simulation. Even in the present model, however, molecules are expected to stop moving outward at some point as the size of the SAM approaches experimental one (nearly micrometer). For a SAM of experimental size, a pushing initiated at the center needs to propagate over a long distance to the periphery. It is then reasonable to expect that the consecutive pushing exists within a certain distance from its origin. Beyond that distance, molecules might opt for diffusing on top of the bottom layer as in the hopping down model. Therefore, despite the absence of chemisoption, molecules in the present model are expected to stop after they travel over some distances. It, however, needs a further investigation to determine whether a large SAM grows through the pushing, hopping down, or a combination of both.

Acknowledgment. This work was supported by the Korea Research Foundation Grant funded by the Korean Government (MOEHRD, Basic Research Promotion Fund) (Grant Nos. 2005-070-C00065 and 2008-521-C00123).

References and Notes

(1) Mirkin, C. A. *ACS Nano* **2007**, *1*, 7.
(2) Salaita, K.; Wang, Y.; Mirkin, C. A. *Nat. Nanotechnol.* **2007**, *2*, 45.
(3) Ginger, D. S.; Zhang, H.; Mirkin, C. A. *Angew. Chem., Int. Ed.* **2004**, *43*, 30.
(4) Jang, J.; Hong, S.; Schatz, G. C.; Ratner, M. A. *J. Chem. Phys.* **2001**, *115*, 2721.
(5) Jang, J.; Schatz, G. C.; Ratner, M. A. *Phys. Rev. Lett.* **2003**, *90*, 156104.
(6) Lee, N. K.; Hong, S. *J. Chem. Phys.* **2006**, *124*, 114711.
(7) Manandhar, P.; Jang, J.; Schatz, G. C.; Ratner, M. A.; Hong, S. *Phys. Rev. Lett.* **2003**, *90*, 115505.
(8) Cho, N.; Ryu, S.; Kim, B.; Schatz, G. C.; Hong, S. *J. Chem. Phys.* **2006**, *124*, 024714.
(9) Sheehan, P. E.; Whitman, L. J. *Phys. Rev. Lett.* **2002**, *88*, 156104.
(10) Weeks, B. L.; Noy, A.; Miller, A. E.; De Yoreo, J. J. *Phys. Rev. Lett.* **2002**, *88*, 255505.
(11) Peterson, E. J.; Weeks, B. L.; De Yoreo, J. J.; Schwartz, P. V. *J. Phys. Chem. B* **2004**, *108*, 15206.
(12) Schwartz, P. V. *Langmuir* **2002**, *18*, 4041.
(13) Salaita, K.; Amarnath, A.; Maspoch, D.; Higgins, T. B.; Mirkin, C. A. *J. Am. Chem. Soc.* **2005**, *127*, 11283.
(14) Hampton, J. R.; Dameron, A. A.; Weiss, P. S. *J. Phys. Chem. B* **2005**, *109*, 23118.
(15) Rozhok, S.; Piner, R.; Mirkin, C. A. *J. Phys. Chem. B* **2003**, *107*, 751.
(16) Rozhok, S.; Sun, P.; Piner, R.; Lieberman, M.; Mirkin, C. A. *J. Phys. Chem. B* **2004**, *108*, 7814.
(17) Ahn, Y.; Hong, S.; Jang, J. *J. Phys. Chem. B* **2006**, *110*, 4270.
(18) Heo, D. M.; Yang, M.; Hwang, S.; Jang, J. *J. Phys. Chem. C* **2008**, *112*, 8791.
(19) Deladi, S.; Tas, N. R.; Berenschot, J. W.; Krijnen, G. J. M.; de Boer, M. J.; de Boer, J. H.; Peter, M.; Elwenspoek, M. C. *Appl. Phys. Lett.* **2004**, *85*, 5361.
(20) Allen, M. P.; Tildeseley, D. J. *Computer Simulation of Liquids*; Oxford University Press: New York, 1987.
(21) Zhang, L.; Jiang, S. J. C. *Chem. Phys.* **2002**, *117*, 1804.
(22) Zhou, J.; Lu, X.; Wang, Y.; Shi, J. *Fluid Phase Equilib.* **2000**, *172*, 279.
(23) Alves, C. A.; Smith, E. L.; Porter, M. D. *J. Am. Chem. Soc.* **1992**, *114*, 1222.
(24) Zhang, L.; Balasundaram, R.; Gehrke, S. H.; Jiang, S. *J. Chem. Phys.* **2001**, *114*, 6869.
(25) Zhang, L.; Goddard, W. A., III.; Jiang, S. *J. Chem. Phys.* **2002**, *117*, 7342.
(26) Berendsen, H. J. C.; Postma, J. P. M.; van Gunsteren, W. F.; DiNola, A.; Haak, J. R. *J. Chem. Phys.* **1984**, *81*, 3684.
(27) John, N. S.; Kulkarni, G. U. *J. Nanosci. Nanotechnol.* **2007**, *7*, 977.
(28) Giam, L. R.; Wang, Y.; Mirkin, C. A. *J. Phys. Chem. A* **2009**, *113*, 3779.
(29) Jarvil, T. T.; Kuronen, A.; Hakala, M.; Nordlund, K.; van Duin, A. C. T.; Goddard, W. A.; Jacob, T. *Eur. Phys. J. B* **2008**, *66*, 75.

JP903254P